J. Fluid Mech. (2002), *vol.* 453, *pp.* 371–394.
DOI: 10.1017/S0022112001007054 Printed in the United Kingdom

The propagation of a gravity current into a linearly stratified fluid

By T. MAXWORTHY[1,2]†, J. LEILICH[2,3], J. E. SIMPSON[1] AND E. H. MEIBURG[4]

[1]Department of Applied Mathematics and Theoretical Physics, University of Cambridge, Silver Street, Cambridge CB3 9EW, UK

[2]Department of Aerospace and Mechanical Engineering, University of Southern California, Los Angeles, CA 90089-1191, USA

[3]Lehrstuhl für Strömungsmechanik, Friedrich-Alexander Universität, Erlangen-Nürnberg, 91058, Germany

[4]Department of Mechanical and Environmental Engineering, University of California-Santa Barbara, Santa Barbara, CA 93106, USA

(Received 15 March 2001 and in revised form 10 September 2001)

The constant initial speed of propagation (V) of heavy gravity currents, of density ρ_C, released from behind a lock and along the bottom boundary of a tank containing a linearly stratified fluid has been measured experimentally and calculated numerically. The density difference, bottom to top, of the stratification is $(\rho_b - \rho_0)$ and its intrinsic frequency is N. For a given ratio of the depth of released fluid (h) to total depth (H) it has been found that the dimensionless internal Froude number, $Fr = V/NH$, is independent of the length of the lock and is a logarithmic function of a parameter $R = (\rho_C - \rho_0)/(\rho_b - \rho_0)$, except at small values of h/H and R close to unity. This parameter, R, is one possible measure of the relative strength of the current $(\rho_C - \rho_0)$ and stratification $(\rho_b - \rho_0)$. The distance propagated by the current before this constant velocity regime ended (X_{tr}), scaled by h, has been found to be a unique function of Fr for all states tested. After this phase of the motion, for subcritical values of Fr, i.e. less than $1/\pi$, internal wave interactions with the current resulted in an oscillation of the velocity of its leading edge. For supercritical values, velocity decay was monotonic for the geometries tested. A two-dimensional numerical model incorporating a no-slip bottom boundary condition has been found to agree with the experimental velocity magnitudes to within $\pm 1.5\%$.

1. Introduction

The subject of gravity current motion, dynamics and structure is a relatively old one with many applications to industrial and natural flows, as discussed in the monographs by Simpson (1997) for example. The background for the present experiments is discussed briefly in these reviews. Here we present a more complete set of new results but also include some of the older ones to be found in these monographs and the original experiments from which they were derived (Simpson 1997, §§ 13.2.1. and 13.2.2.). Also, numerical modelling is carried out in two dimensions with a no-slip condition at the bottom boundary. A dimensionless parameter is introduced that incorporates the dependence of the motion on the current density and the ambient

† Author to whom correspondence should be addressed.

stratification. At the same time the aspect ratio [length (L)/height (h)] of the volume of released fluid does not appear to be a relevant parameter, at least for the range of studied here. Results are presented from which it is possible to calculate the speed of propagation for all combinations of the relevant independent variables.

As background for the present stratified cases we discuss first the 'classical' case, i.e. the propagation of gravity currents, from fixed volume releases, along the horizontal floor of a tank of height, H, containing a homogeneous fluid of density, ρ_A. Basic knowledge of these commonly observed entities is summarized well in the reference given above supplemented by more detailed commentary in Simpson (1972), Britter & Simpson (1978, 1981), Simpson & Britter (1979), Huppert & Simpson (1980) and Rottman & Simpson (1983) for example. The initial volume of heavy fluid, of density, ρ_C, has the shape of a right parallelepiped of length, L, height, h, and width, W. Here, based on the results of Rottman & Simpson (1983), after a brief acceleration phase, the velocity of the nose of the current becomes constant for any given experiment at a value, V, given by

$$V = k(g'h)^{1/2}, \tag{1}$$

where $g' = g(\rho_C - \rho_A)/\rho_A, g$ is the acceleration due to gravity and k is a quantity, given in Rottman & Simpson (1983), that depends on h/H. An alternative description gives

$$V = f(\phi)(g'a)^{1/2},$$

where $\phi = a/H$, a is the measured height of the nose of the current and $f(\phi)$ is given in Huppert & Simpson (1980), in which a is designated as h_0.

In this phase of the motion the velocity is controlled by conditions at the nose and the flow is not self-similar. Upon the initial release a wave or bore is generated, on the interface between the current and its surroundings, that propagates backwards, i.e. in a direction opposite to the main current, reflects from the endwall of the channel and then travels, as a wave of depression, towards the nose of the current (Rottman & Simpson 1983). Upon interacting with the nose the wave changes so that its speed of propagation is now given by

$$x \approx t^{2/3} \quad \text{or} \quad V \approx t^{-1/3}.$$

Here x is the distance of the leading edge of the current from the downstream end of the initially dammed section (figure 1) and t the time. In this phase of motion the flow is self-similar and while the Froude number of the nose, scaled on the density difference and a suitable measure of the variable height of the current, is constant it does not control the motion. This is determined by a force balance between the horizontal buoyancy gradient and inertial force associated with the whole current, together with volume conservation (see e.g. Huppert 1982; Didden & Maxworthy 1982). The transition from (1) to this state takes place after the current has travelled a distance of approximately $x/L \approx 10$ (Rottman & Simpson 1983).

Our purpose in what follows is to determine how this sequence is modified when the heavy fluid is released at the lower boundary of a tank containing a linearly stratified ambient fluid; that is, how the internal waves produced by the lock release interact with the current to change its characteristics and how it, in turn, may change the wave field. In one limit, Wu (1969), Schooley & Hughes (1972) and Amen & Maxworthy (1980) released mixed fluid, with the same density as the central layer, at the centre plane of a stratified fluid contained in a long narrow box, and observed the evolution of the resulting current, the internal waves generated and the interaction between the two. In the present case (see above and § 5), except for questions of the

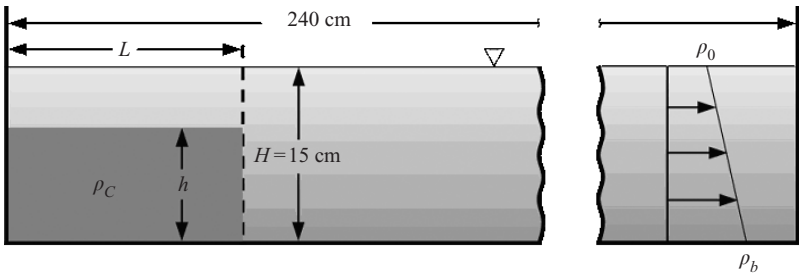

FIGURE 1. Apparatus. Definition of the various geometric quantities used in this study.

subtle differences between slip and no-slip boundary conditions at, and asymmetry about, the centreplane in the former case, this would be equivalent to releasing fluid that has the same density as the bottom of the stratified fluid. In the other limit one might expect that when the density of the release is very much larger than that at the bottom of the stratification the result would be a gravity current that is indistinguishable from a 'classical' current into a fluid with a density equal to the average in the stratified layer. More recently Felix (2000) has presented an analytic solution for leading-edge motion in a stratified fluid; however there appears to be no clear-cut way to relate his solution to the physical situation considered in the present work. Further, gravity current propagation and solitary wave formation at the mid-level of a hyperbolic tangent density distribution was studied by Maxworthy (1980), while Manins (1976) considered a constant inflow into the centreplane of a linearly stratified fluid.

2. Scaling of the gravity current motion in a stratified fluid

The early experiments of Simpson (1997) were run under a variety of different conditions with N varying from 0.74 to 1.99 and a number of different values for the height of the lock (h) and the initial density of the current (ρ_C), while H was kept constant at a value of 15 cm. Here $N^2 = (g/\rho_0)(-\mathrm{d}\rho/\mathrm{d}z) = g(\rho_b - \rho_0)/\rho_0 H$, z is the vertical coordinate, g the acceleration due to gravity, ρ the fluid density and ρ_0 a reference density, in this case that at the surface, $z = H$. In these preliminary experiments there were not enough cases close to any particular value of N to determine the possible parametric dependence of the initial constant velocity (V), as measured by its Froude number (Fr), on this quantity alone, where

$$Fr = V/NH. \tag{2}$$

It was therefore necessary to find a dimensionless ratio that incorporated these quantities and that allowed one to at least reduce the data for a particular lock depth (h) to one curve. Physically, one can justify the final results, to be presented in § 5, by realising that one possible measure of the effective density difference driving the current is $(\rho_C - \rho_0)$, while the magnitude of the stratification is measured by $(\rho_b - \rho_0)$, see figure 1. The ratio between these density differences, R, is then a dimensionless measure of the relative strengths of the current and the stratification:

$$R = (\rho_C - \rho_0)/(\rho_b - \rho_0) = N_C^2/N^2. \tag{3}$$

Here $N_C^2 = g(\rho_C - \rho_0)/\rho_0 H$, so that N_C is a fictitious or effective buoyancy frequency calculated using the density of the fluid initially behind the lock. Other forms for a ratio of the magnitude of forcing to stratification have been tested as well. For

example in (3) any value of reference density between ρ_b and ρ_0, in particular ρ_h, the density at the height h, could have been used to reduce the data. This possibility was tested in Leilich (2000) where a single, separate curve was generated for each value of h/H, as also occurred when using (3). Since no single, simple combination was found to give a complete reduction of the data to a single curve, equation (3) was finally chosen since it gave the most compact and mathematically straightforward data reduction, as will be seen. Note that it is necessary to use the reference height at which the reference density is chosen in defining N_C and N.

One would expect, in the limit of large R, that the current would resemble one propagating into a fluid of density $(\rho_b + \rho_0)/2$. Using the results of Rottman & Simpson (1983) with the density difference given by

$$[\rho_C - (\rho_b + \rho_0)/2]$$

one finds, after some trivial algebra, a Froude number given, for large R, by

$$Fr_{LR} = k\{[h/2H][2R-1]\}^{1/2} \approx k\{[h/H][R]\}^{1/2}, \tag{4}$$

where k is the experimentally determined function of h/H given by Rottman & Simpson (1983) in their figure 9. See equation (1). The values of k used here were taken from a straight line fit to the experimental points on that plot and are, for the values of h/H used here, 1/3, 1/2, 2/3 and 1, are respectively 0.59, 0.55, 0.51 and 0.45. This result, equation (4), will be compared with the experimental results in what follows. Note that the second result given in (4), for R very much greater than unity, is the same as if the current were propagating into a fluid of density ρ_0.

3. Experimental apparatus and procedure

A fluid with a linear density profile was set up in a tank 244 cm long (the x-direction), 20 cm wide (the y-direction) and 30 cm deep (the z-direction), figure 1, using the Oster (1965) method. This method introduces increasingly less dense fluid at the surface through a floating, foam-bottomed diffuser. Thin, constant-density dye layers were placed at various levels within the stratification by introducing the dye into the diffuser when the fluid surface was at appropriate levels. A gravity current of appropriate density was released from behind a lock gate that was either 20 or 40 cm from one end of the tank. The shape and rate of advance of the resultant gravity current were recorded by a combination of still photography and video. In order to reduce parallax effects and provide a larger image the video camera was towed on a carriage at the speed of the front. In the new experiments reported here two values of N (approximately $1.40\,\mathrm{s}^{-1}$ and $1.98\,\mathrm{s}^{-1}$), four values of h/H (1/3, 1/2, 2/3 and 1, while H was, again, kept constant at 15 cm), two values of L (resulting in six values of L/h) and many values of ρ_C were used, in order to check the validity of the scaling given in § 2. A table of all the experimental values and some of the dependent variables is given in Appendix A.

4. Numerical procedure

In order to compare with the experimentally obtained results, we performed high-resolution two-dimensional simulations of the dimensionless system of governing equations in the streamfunction (ψ) and vorticity (ω) formulation in the

Boussinesq limit:

$$\frac{\partial^2 \psi}{\partial x_i \partial x_i} = -\omega, \tag{5a}$$

$$\frac{\partial \omega}{\partial t} + u_i \frac{\partial \omega}{\partial x_i} = \frac{1}{\sqrt{Gr}} \frac{\partial^2 \omega}{\partial x_i \partial x_i} - \frac{\partial \rho}{\partial x_1}, \tag{5b}$$

$$\frac{\partial \rho}{\partial t} + \frac{\partial (\rho u_i)}{\partial x_i} = \frac{1}{\sqrt{GrSc^2}} \frac{\partial^2 \rho}{\partial x_i \partial x_i}. \tag{5c}$$

All terms in the equations have been made dimensionless using the channel height H, the density at the surface, ρ_0 and the velocity scale NH, and the summation convention has been used. Gr is the Grashof number NH^3/v, a measure of the ratio between buoyancy forces and viscous forces, and Sc is the Schmidt Number v/D. Here D is the coefficient of molecular diffusivity and v the kinematic viscosity, ρ the local dimensionless density of the fluid, u_i the dimensionless fluid velocity vector and x_i the dimensionless Cartesian coordinate axes. Since the computations were carried out in two dimensions only values of i of 1 and 2 were used.

No-slip boundary conditions were specified along the lower and upper walls. The vertical endwalls, however, did allow for slip, thereby enabling the employment of Fourier series expansions of the variables in the horizontal direction. Tests performed by Härtel, Meiburg & Necker (2000) have demonstrated that this slip condition does not affect the front until it has approached the endwall to within less than one channel height. The nonlinear terms were evaluated in a pseudo-spectral manner at each time level, cf. Canuto *et al.* (1988). In the vertical direction, sixth-order compact finite differences (Lele 1992) were utilized. Time integration was fully explicit and employed the third-order low-storage Runge–Kutta scheme developed by Wray (1991). The simulations were initialized with the fluid at rest, while the nominal discontinuities in the initial concentration field were approximated by smooth error function profiles. Further details regarding the numerical implementation as well as the validation of the code can be found in Härtel *et al.* (2000).

Height ratios h/H of 1/3, 1/2, 2/3 and 1 were simulated. To determine the relationship between Froude number and the density ratio R this latter parameter was varied between 1 and 3 in steps of 0.5. For these simulations only the first quarter of the channel (i.e. $x = \pm 4$) was simulated as the stage of constant velocity was reached very fast after the 'lock release' and the simulation time could be abbreviated. As the distance between the front and the end boundary was generally greater than $\Delta x = 3$ the relative error in the front speed was well below 10^{-4} as determined by Härtel *et al.* (2000). This meant that the simplification of shortening the channel to decrease the computational time had no significant influence on the results. However, the wave which eventually propagated ahead of the current reached the end of the channel and was reflected. The simulation ended well before the reflected wave reached the gravity current front.

For these simulations the grid had either $2.6 \times 10^5 (1024 \times 256)$ grid points or more than 10^6 (2048×512) depending on the Grashof number. The Grashof number was calculated and applied to the simulation as an initial condition. The simulations were generally performed at values of the dimensionless parameters as if the fluid were water and $N = 1.40\,\mathrm{s}^{-1}$. Thus, the Grashof number varied from about $Gr = 1.2 \times 10^8$ to $Gr = 3.4 \times 10^8$. A value of $Sc = 1$ was used throughout. While this was much smaller than the experimental value, it was employed in order to avoid resolving the

very narrow concentration boundary layers. This choice was justified on the basis of tests performed by Härtel *et al.* (2000), which showed that an increase in Sc above unity led to very minor changes in the flow dynamics.

In the simulations with the total channel length, a grid of more than 10^6 grid points was used (4096×256). For the simulations with higher Grashof number this grid was too coarse to give a stable solution. As a simulation with half the grid width would have taken more than a month on the available workstations it was decided to perform the simulation at a lower Grashof number. Compared to the results gained with the higher Gr it was found that using a lower Grashof number of about 0.75×10^8 influenced the results for the front speed by less than 1%. This error was assessed to be acceptable in order to obtain results for the generation of internal waves and wave–gravity current interaction.

As mentioned above, to avoid discontinuities in the density field a diffusive boundary layer was implemented between gravity current and ambient field. Therefore the position of the front was assumed to be at the point where the local density had a value of 85% of the assigned gravity current density.

5. Results

Thirty six experiments were run for the two values of N and four values of h/H mentioned above and numerous values of ρ_C. In a few cases the length of the lock (L) was doubled from 20 to 40 cm (see Appendix A). Some of the older data found in Simpson (1997) were used also. In all cases the Reynolds numbers, based on the height of the gravity current head, were large enough that viscous effects were not important based on previous experience with the non-stratified case.

Figures 2, 3 and 4 show photographic sequences of the current and wave-field evolution under different but representative initial conditions. Figures 2 and 3 were taken from video sequences and show the flow evolution for large and small values of R, respectively.

Figure 2 is the most straightforward to describe. As will be shown in detail later, the gravity current is moving at a value of Fr greater than $1/\pi = 0.318$, that is it has an initial velocity that is faster than that of the linear, mode-one, long wave in the wave guide, i.e. (NH/π). This state is usually referred to as being 'supercritical' (Long 1955). The head of the current and the wave are locked together and there is no obvious wave generation behind the head. In the case shown here the initial Fr is 0.438. This velocity is maintained for a distance of approximately $16h$ (see below), and thereafter begins to slow. The Froude number becomes 'critical', i.e. $Fr = 1/\pi$, at frame 602. Then as the current slows further the wave field begins to slowly separate from the current head and move upstream. By frame 902 (where the position of the leading edge of the current, x, is 155 cm and the time, t, is 22 s after initiation) there is the slightest suggestion of a second, weak wave forming downstream of the head. This sequence was typical of runs for which the initial Fr was supercritical in this relatively short tank.

Figures 3 and 4 are typical of the evolution for an initial Fr that is 'subcritical', i.e. $Fr < 1/\pi$. In figure 3 the value of Fr is 0.264 and in figure 4 it is 0.203. In figure 3 the initial velocity is constant for a short distance (until frame 576, where the value of x at which a deviation from a constant velocity occurs, X_{tr}, is 75 cm and the equivalent time, T_{tr}, is 10.5 s) (the exact definitions of X_{tr} and T_{tr} are discussed below). The initial x versus t trajectory is shown as one of the curves of figure 5, and a more detailed one is shown in figure 6. Within a short time (frame 516 in figure 3) a second

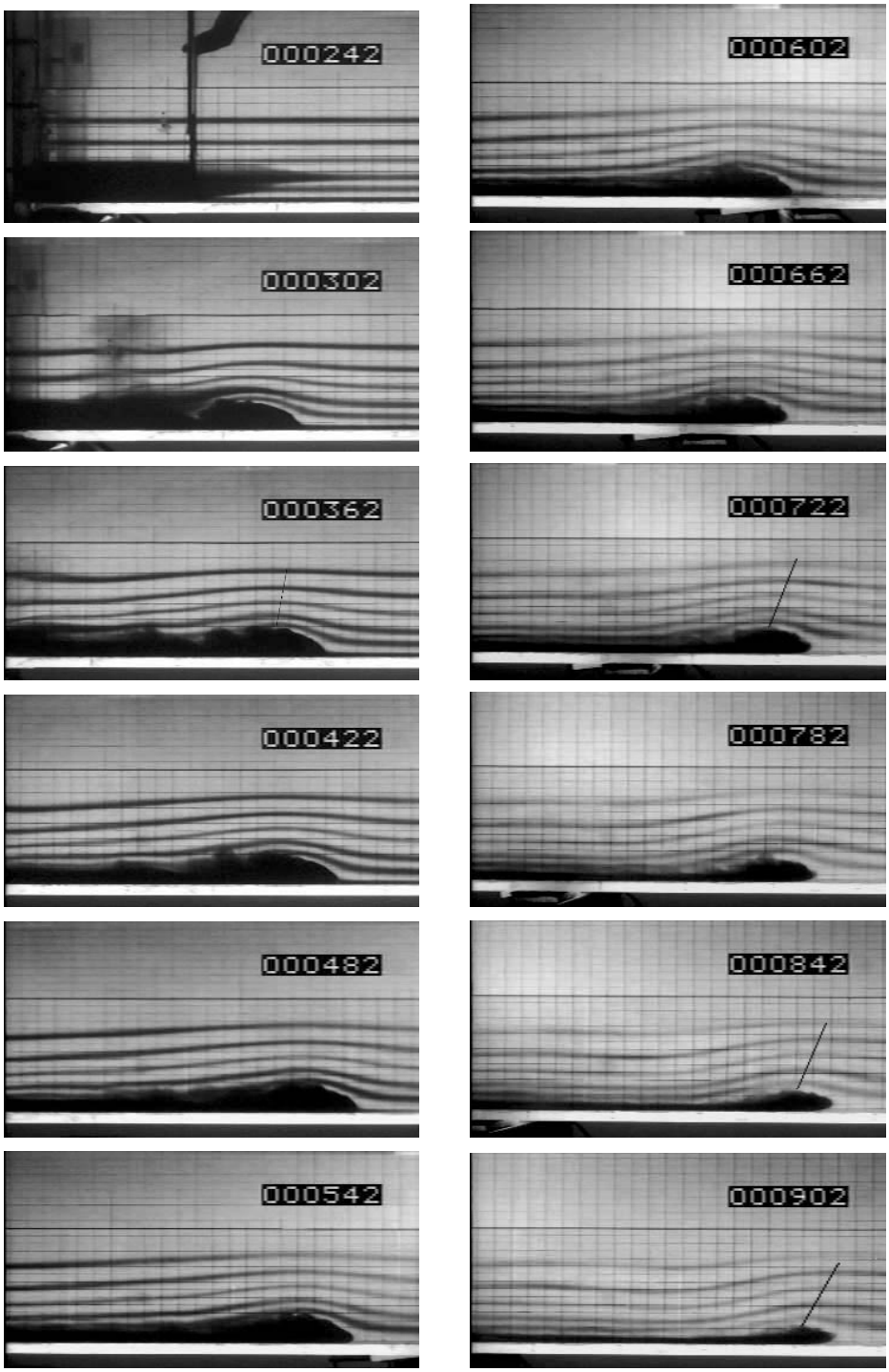

FIGURE 2. A time sequence of images taken from a video recording of a supercritical gravity current propagation. Run 6, $Fr = 0.438$. The images are 60 frames or 2 s apart and run down the left column followed by the right. The black lines join the points of maximum height on each isopychnal, i.e. they are lines of constant phase.

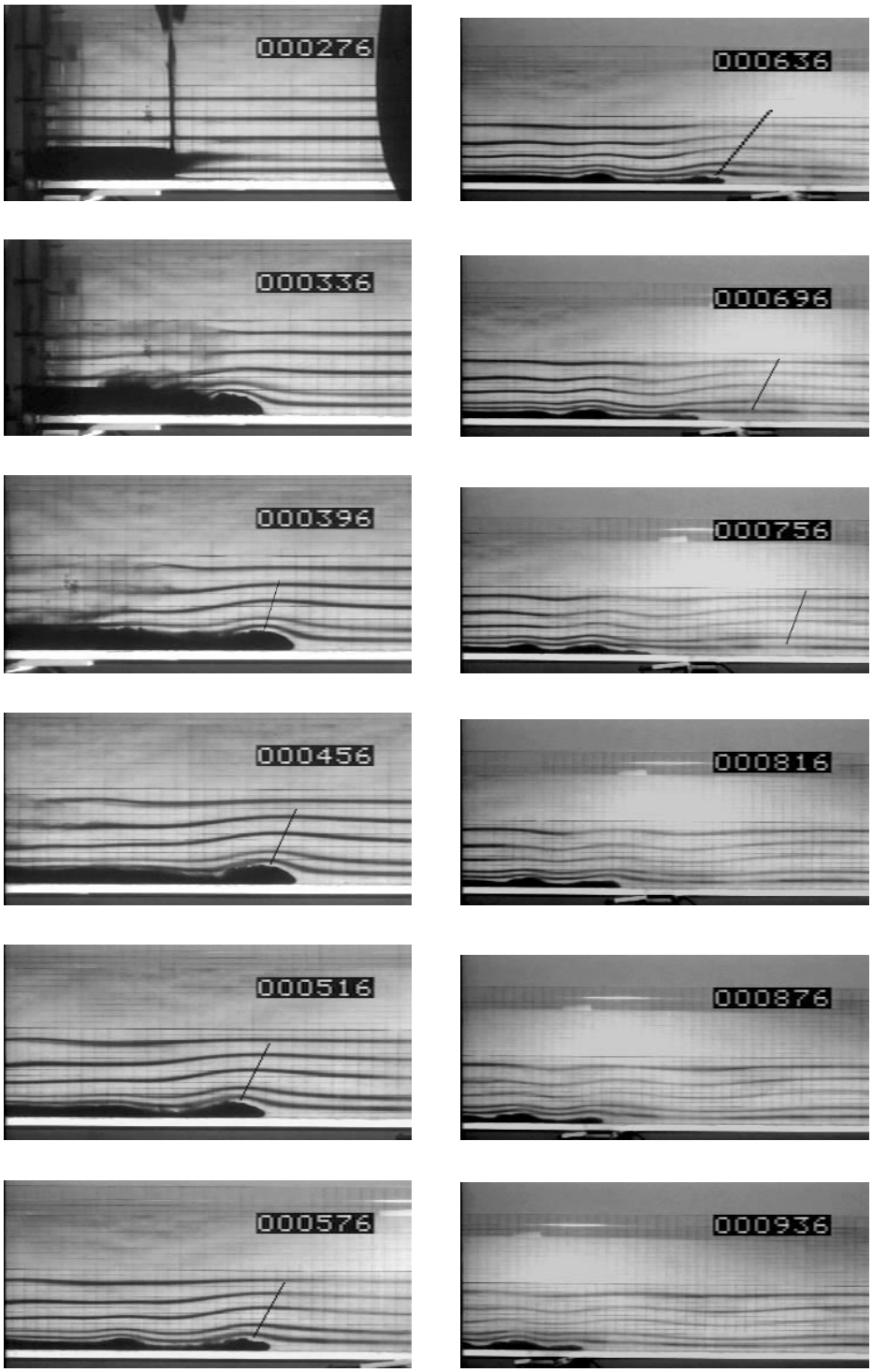

FIGURE 3. The same as figure 2 but it shows subcritical propagation. Case 19, $Fr = 0.264$.

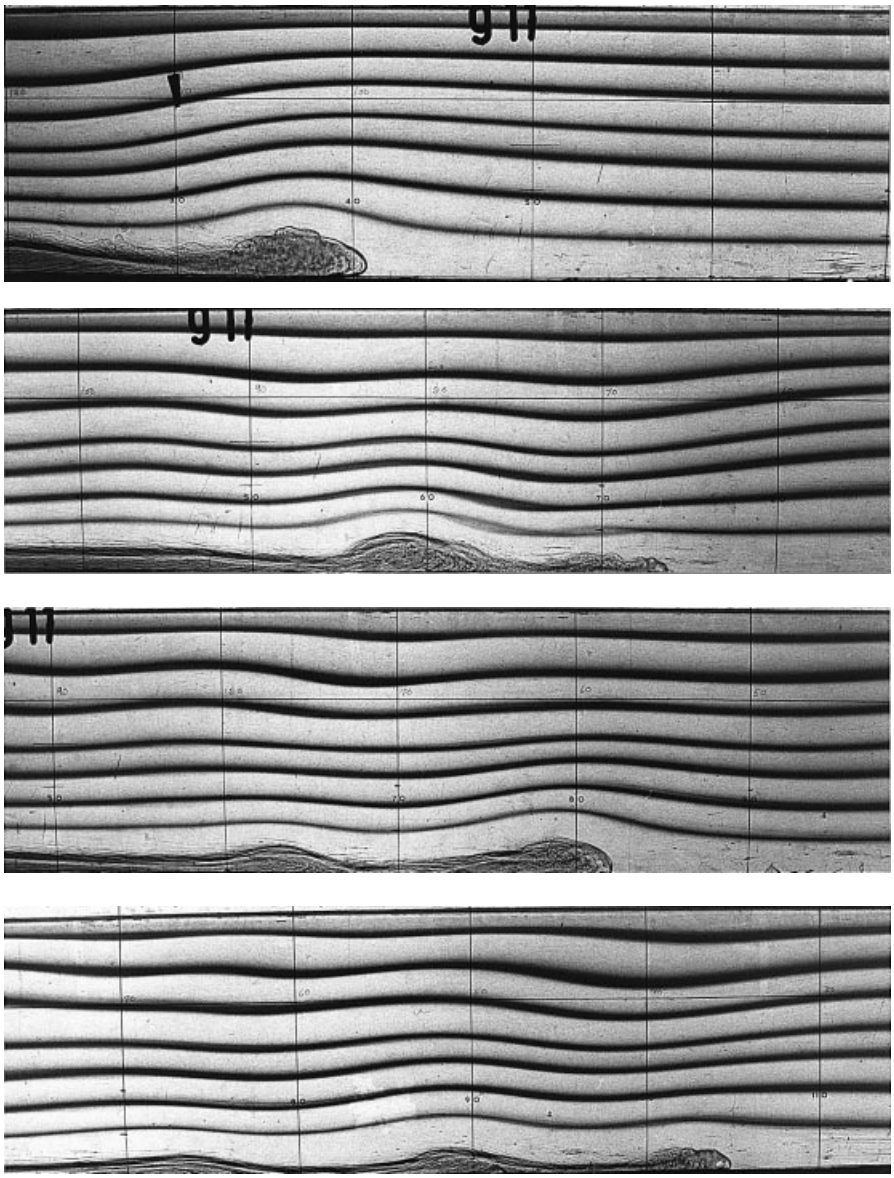

FIGURE 4. A time sequence of original photographs of a subcritical case with a value of Fr of 0.203, showing details of the head structure and the waves generated by the gravity current motion. In particular note the absence of strong mixing behind the head and in the main body of the current.

wave begins to form behind the first. This quickly grows in amplitude and interacts back onto the current to form a second elevation of the dyed fluid. During this event the lines of constant phase of the first wave have been tilting forward, indicating a propagation of energy upstream, and by frame 636 it has begun to leave the current head behind. Now the trough following the first wave of elevation interacts with the current to slow and eventually stop it. The next wave, and its associated crest in the current, now moves forward, followed by a third wave, and by frame 816 the second wave crest has reached and reinforced the nose of the current so that the latter begins to move forward again. This sequence is repeated as the faster propagation of the

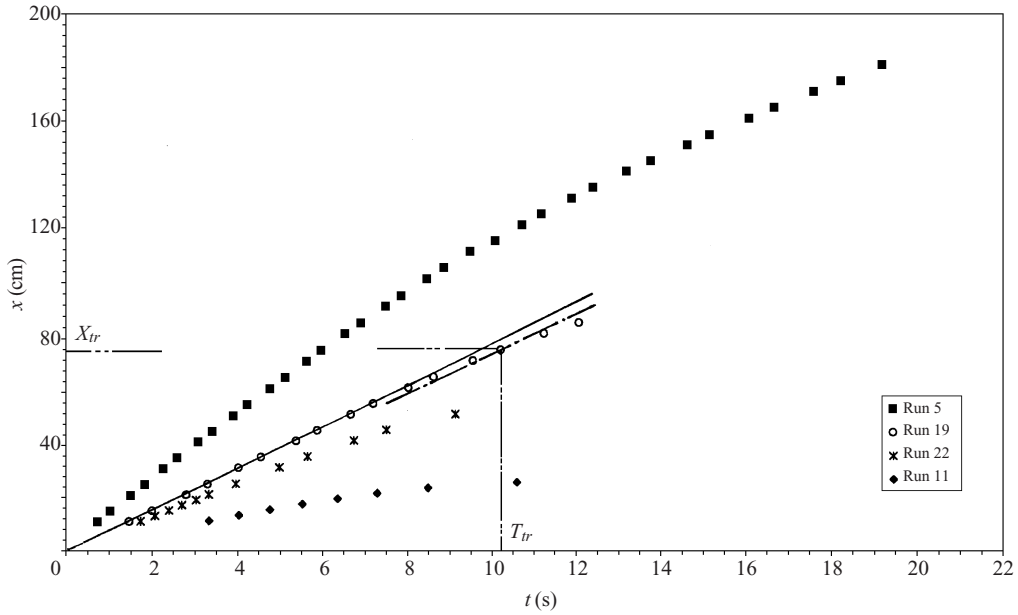

FIGURE 5. x versus t diagrams of the noise position for four cases. For Run 19 the definitions of X_{tr} and T_{tr} are indicated.

second trough slows and stops the nose again (frame 936) followed by a new forward motion initiated by the arrival of the third wave crest (frame 1056). A plot of x versus t for this complex interaction of current and waves to be found in figure 6. Here, as described above, the trajectory of the nose of the gravity current is seen to come almost to rest as it interacts with the troughs of the waves generated by its motion. The velocity of all the waves thus formed increases as they separate from the current, with the first moving at a speed close to that of the mode-one long wave (NH/π). All the trailing waves have almost identical speeds but the values are less than that of the first wave crest.

Figure 4 shows the structure of the flow in more detail and in particular that of the gravity current itself. It is the sequence from which figure 13.18 of Simpson (1997) was taken. It shows how the current and the waves produced by its release interact at a low value of R. In the first photograph of this sequence the current head and first wave are propagating together but the wave is slowly moving ahead. In the second the wave has separated from the current and the first trough is slowing the current head. Figure 13.18 of Simpson (1997) fits between these two images. By the third photograph the second wave has engulfed the leading head and the current begins to move forward again. Finally this too slows and is caught by the next wave.

The details of the initial motion for four cases are shown in figure 5. On this figure is also shown the manner in which the transition distance (X_{tr}) and time (T_{tr}) were defined. The chain-dotted straight line has a slope that is 95% of the initial velocity, 7.69 cm s^{-1} in experiment 19. The point where this line intersects the curve of x versus t was considered to be the coordinates of the required transition values. As long as one was consistent in the application of this criterion it was then possible to determine the parametric dependence of these transition values.

From plots like those of figure 5 one can determine the initial velocity and hence Fr for all cases. The numerical values are given in Appendix A and they are plotted

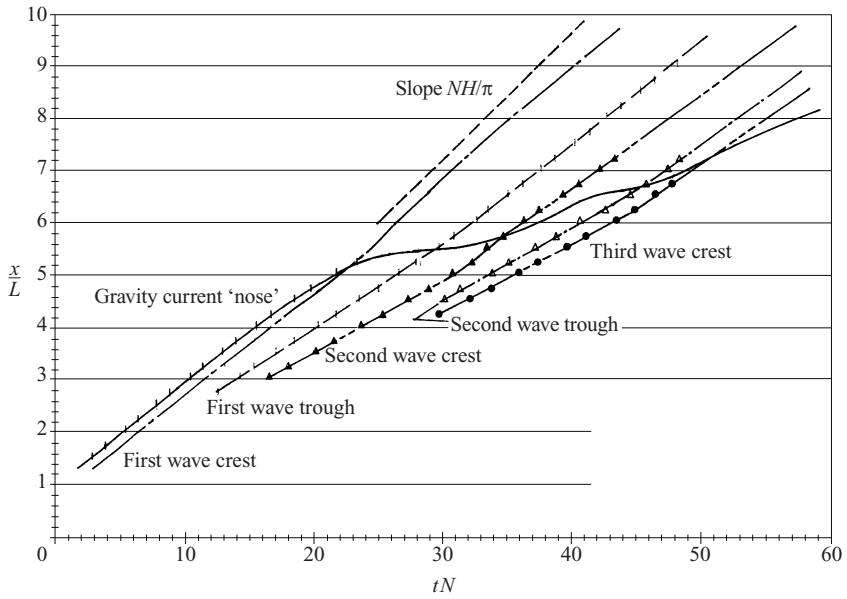

FIGURE 6. A detailed study of the positional history (x/L versus Nt) of the gravity current nose and three of the waves generated by its release. The maximum and minimum vertical excursions of the second isopycnal from the bottom of figure 3 were used to indicate the positions of the waves. For clarity many of the points that were used to construct this plot have been omitted. The oscillatory progress of the nose is clearly demonstrated as it interacts with the internal waves created by its motion. The speed of the mode-one long wave is plotted as NH/π. Case 19. $N = 1.941\,\mathrm{s}^{-1}$, $Fr = 0.264$, $R = 1.397$.

on figure 7 as a function of R. As was to be expected, Fr increases with both R and h/H. The scaling used here, i.e. R, removes the direct dependence on N but not on h/H. Also, varying L/h by a factor of two on any one curve produces points that deviate from the fit by no more than the general trend. As noted on the figure, each curve is represented well by the relationship

$$Fr = C + K \log_{10} R. \tag{6}$$

For all the curve fits shown here the correlation coefficient is between 0.997 and 1. However, note a slight deviation for the two lower values of h/H and R close to unity. The values of C and K for each curve are given on figure 7. It is now possible to plot C and K as functions of h/H and these are shown on figures 8(a) and 8(b). It is impossible to choose between these two ways of plotting the results. In the first (figure 8a) one finds

$$C = a + b \log_{10}(h/H), \tag{7}$$

and

$$K = c + d \log_{10}(h/H). \tag{8}$$

In the second (figure 8b)

$$C = f(h/H)^g, \tag{9}$$

and

$$K = m(h/H)^n. \tag{10}$$

For the experimental data: $a = 0.270$, $b = 0.246$, $c = 0.935$ and $d = 0.307$ while

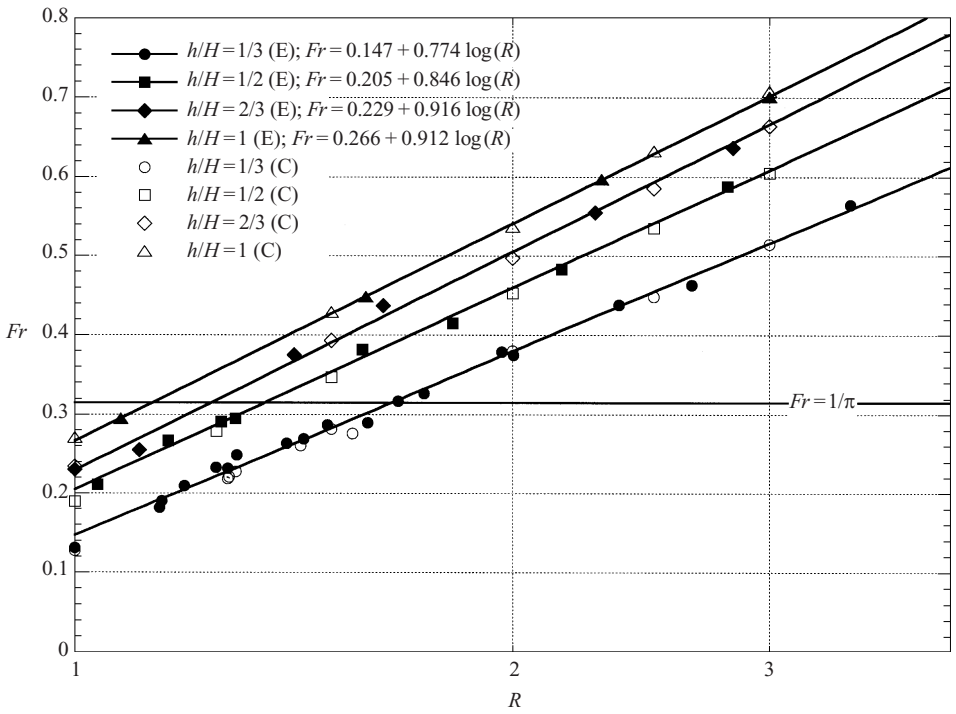

FIGURE 7. Fr versus R for all the experiments and computations performed during this study. Here an E and solid symbols represent the experiments and a C and an open point the computations. Errors are of the order of the deviations of the points from the fitted straight lines.

$f = 0.277$, $g = 0.530$, $m = 0.938$ and $n = 0.157$. In all cases the correlation coefficient of each curve fit is between 0.92 and 0.99. Using either of these sets of functions it is possible, in principle, to reduce all the curves of figure 7 to one straight line on a semi-logarithmic plot. However, the functional relationships given above are really all that are needed to calculate Fr for any combination of R and h/H. Similar results have been found for the numerical data and these are treated in what follows. Further comments on these results are to be found in § 5.

Numerical solutions for sub- and super-critical conditions that are broadly equivalent to figures 3 and 4 are shown in figures 9 and 10. It can be seen that many of the characteristics of these solutions are similar to those found in the laboratory experiments. The major difference is in the details of the turbulent structures behind the head. In the two-dimensional numerical solutions these cannot evolve further into three-dimensional turbulence and hence maintain a characteristic Kelvin–Helmholtz vortex morphology with concommitant entrainment into the body of the current. Also, the spanwise 'lobe and cleft' structure seen at the head of the current in the experiments must be missing in the numerical solutions. Despite these differences the numerical x versus t trajectories give initial velocities that are virtually identical to those measured from the experiments. These are indicated by the open symbols on figure 7. To avoid confusion the curve fits for these points are not given on the figure but they also have the logarithmic form given to equation (6). The corresponding values of C and K, for the four values of h/H considered, are plotted on figures 8(a) and 8(b) and in this case too either a logarithmic or a power-law fit to the

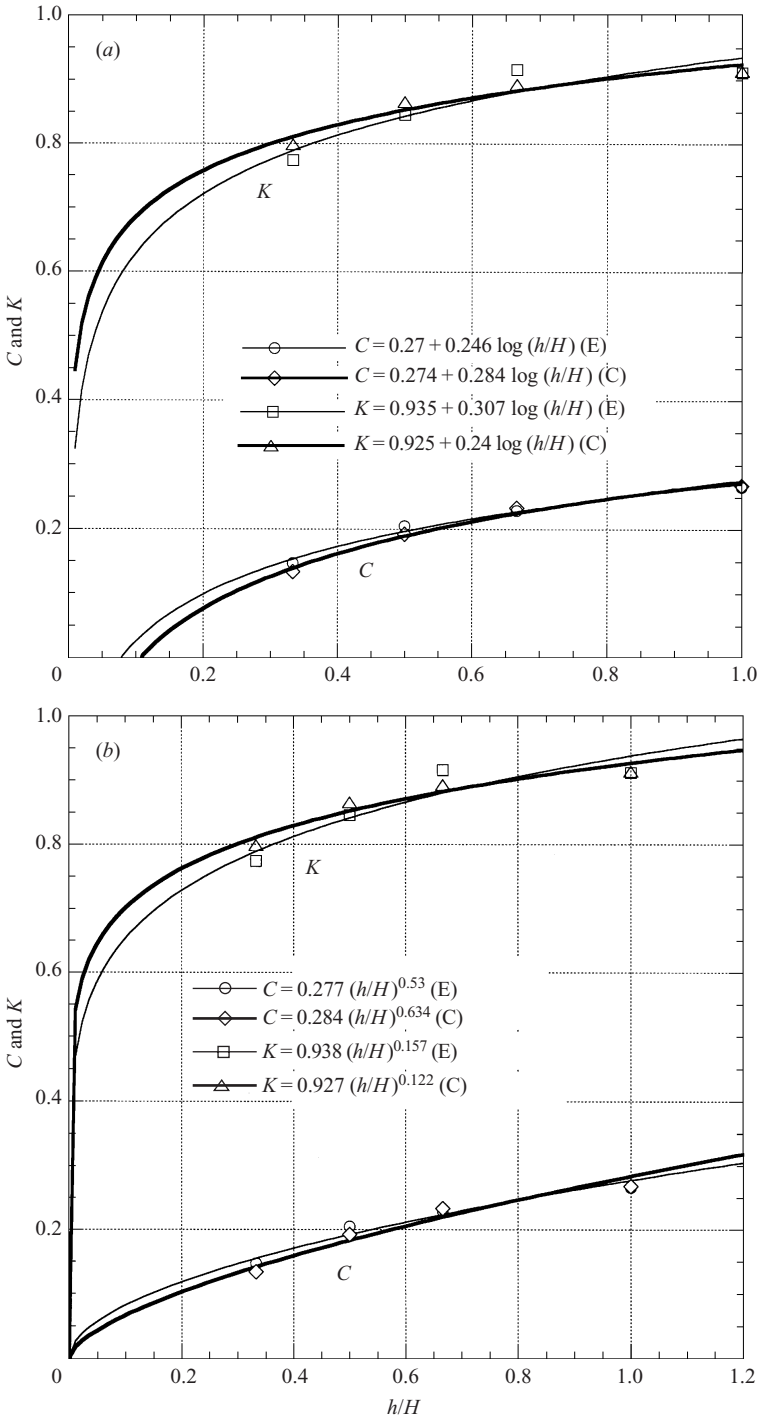

FIGURE 8. C and K versus h/H for the both the experiments (E) and computations (C): (*a*) a logarithmic fit to the data, (*b*) a power-law fit to the data.

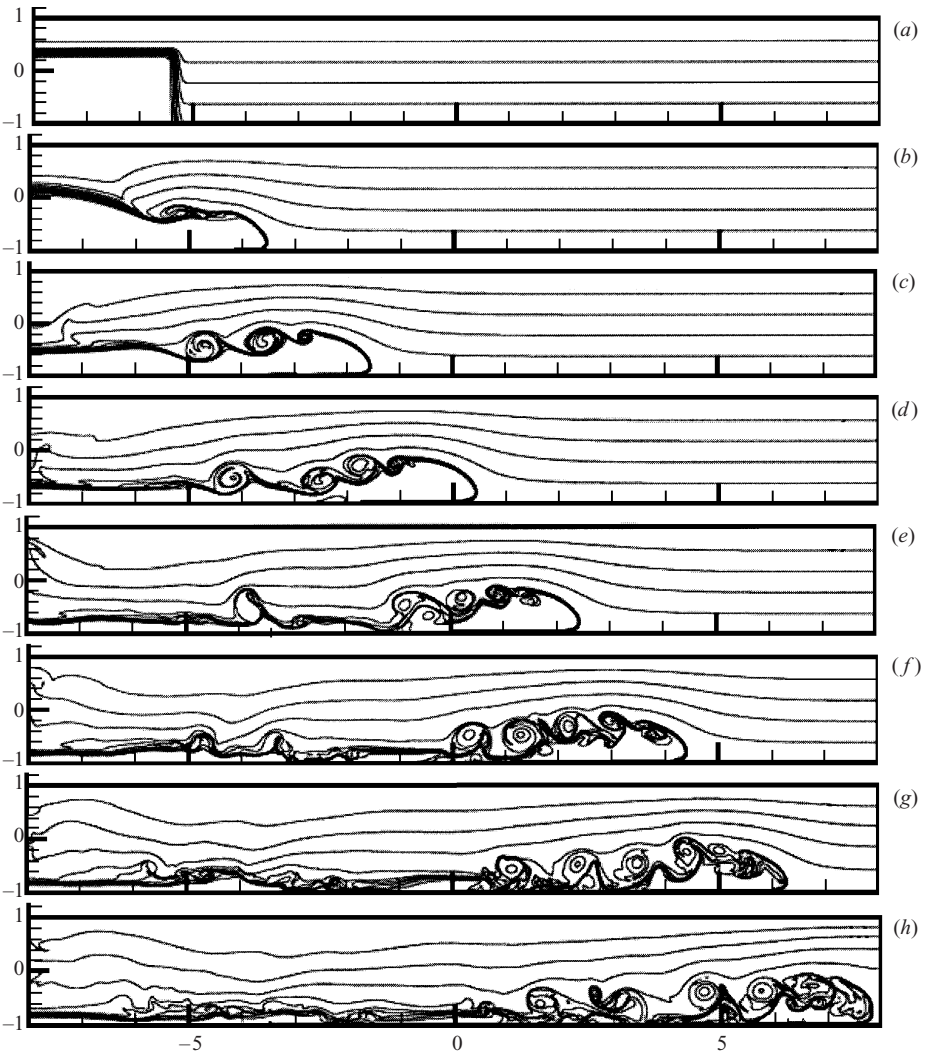

FIGURE 9. Sequence of density fields for a supercritical simulation. Here and in figure 10 the vertical and horizontal axes are made dimensionless with $H/2$. $Fr = 0.489$, $h/H = 2/3$. The time between frames is 0.90 s, $N = 1.981\,\mathrm{s}^{-1}$ and $H = 15$ cm.

data is justified, but see § 5. For the numerical data, $a = 0.274$, $b = 0.284$, $c = 0.925$, $d = 0.240$, $f = 0.284$, $g = 0.634$, $m = 0.927$ and $n = 0.122$ in equations (7)–(10).

Comparison between the laboratory experiments and the limiting result for large R (i.e. Fr_{LR}, equation (4)) is presented in figure 11. There, as might be expected, agreement is best at large R except for the case of $h/H = 1/3$, where it seems that the two curves will asymptote to one another beyond the range of R covered here. For the two larger values of h/H equation (4) is a good approximation to the actual values of Fr for R as small as 2.0. The trend with h/H suggests that for very small values the approximation of equation (4) will never be adequate and that, most likely, some other formulation must be used.

As shown on figure 5 the constant-velocity phase lasted a finite time or distance. Assuming that this phase could be considered terminated when the average velocity

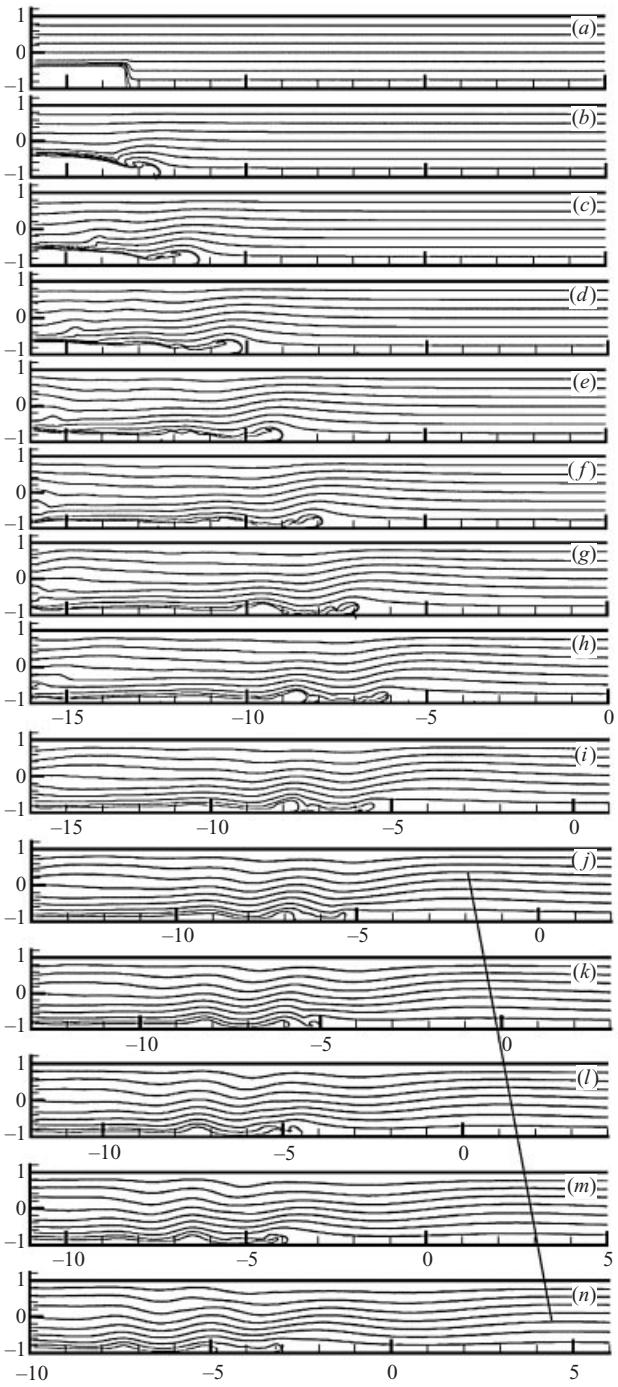

FIGURE 10. Sequence of density fields for a subcritical simulation. $Fr = 0.219, h/H = 1/3$. The time between frames is 1.80 s, $N = 1.468\,\mathrm{s}^{-1}$ and $H = 15\,\mathrm{cm}$. The line crossing the last 5 frames is an attempt to indicate the propagation of the first mode-one wave to be released by the current with $Fr = 0.308$ which is approximately equal to $1/\pi = 0.318$.

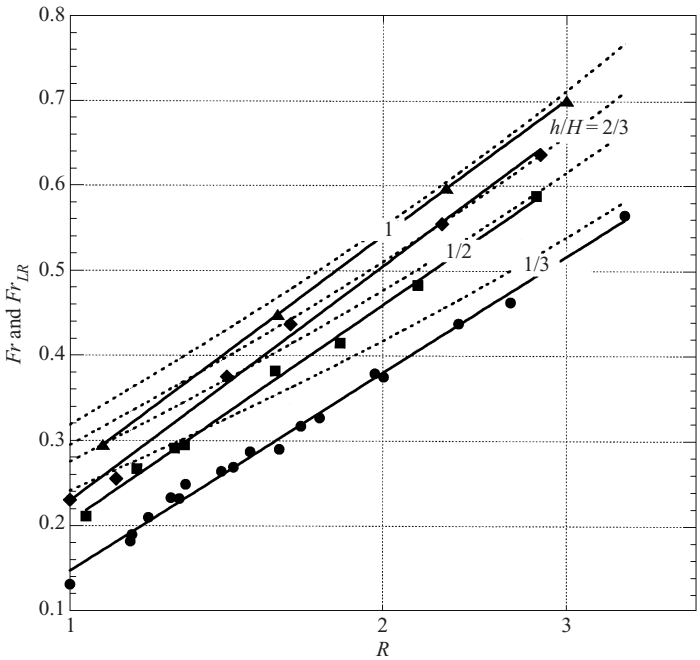

FIGURE 11. Comparison between the experimental results for Fr versus R and equation (4) which is thought to describe the behaviour for large R. The solid lines and points are the experiments and the dotted line equation (4) for the various values of h/H.

since inception was 95% of the maximum velocity it was possible to measure X_{tr} and T_{tr} (figure 5) for all experiments. These results could be plotted in two ways. The first, and most obvious, was to plot the dimensionless X_{tr} and T_{tr} versus the true independent variable R. The clear-cut way to make T_{tr} dimensionless was to form the product NT_{tr}. However there were two ways to make X_{tr} dimensionless, i.e. to divide by either h or H. The best choice will be introduced in what follows. Plotting NT_{tr} directly against the independent variable R resulted in separate curves for the four values of h/H. Each had a maximum close to the value of R at which $Fr = 1/\pi$, i.e. at which the flow was critical. This result suggested that a plot of NT_{tr} vs. Fr would be more useful, even though Fr is a dependent variable, and this turned out to be correct. Then, further data manipulation shows that it is possible to reduce the resulting four curves to one by plotting $NT_{tr}H/h$ vs. Fr, figure 12. Here, also, the maximum occurs close to the critical state. for subcritical states $NT_{tr}H/h$ tends to zero as Fr decreases, while for the supercritical states it is decreasing as Fr increases. Using the insight gained from this exercise one can make further progress by plotting X_{tr}/h vs. Fr, since using the length scale h turns out to be the best way to make X_{tr} dimensionless. Using H results in four distinct curves while h suggested here gives only one (figure 13). Here, for supercritical flows X_{tr}/h is constant, at a value of 16 ± 3, while it increases for increasing subcritical Fr. Further comment on these results is given in § 5.

Simpson (1997) hypothesized that the combined flow of gravity current and internal wave, as outlined above, was similar to the stratified flow over a solid object, as studied by Long (1955). In the latter the internal wavelength (λ) between the first two wave crests generated by stratified flow over an object was defined and a theoretical

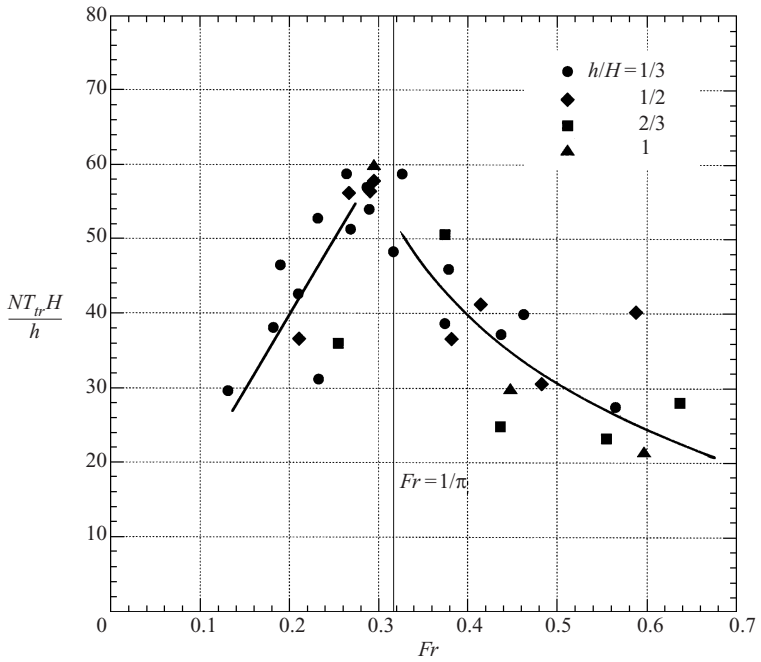

FIGURE 12. The dimensionless transition time, $NT_{tr}H/h$, versus the dependent variable Fr. The solid lines have been added as a visual guide to the reader in order to show the data trend.

expression derived as a function of Fr:

$$(\lambda/H)_L = 2\pi/(Fr^{-2} - n^2\pi^2)^{1/2}, \tag{11}$$

where n is the vertical mode number and the subscript L indicates that this is Long's (1955) result. The definition of λ for the present case is shown on the inset on figure 14. This quantity was measured for all cases where an obvious second wave crest could be identified before the conclusion of the experiment, i.e. before the first wave reflected from the endwall and interacted back with the advancing current. The results are shown in figure 14 for both the present experiments and computations, and the experiments of Simpson (1997). A curve identifying equation (11), for $n = 1$, is included for comparison. The chain-dotted curve is added as a guide to visualization of the trend and is given, approximately, by $[\lambda/H]_L/2$.

Long (1955) also defined, for stratified flow over an obstacle of finite height a, regions in $[Fr, a/H]$ space where such waves, with various vertical mode numbers, should be excited. These regions are shown in figure 15 together with the measurements from Simpson (1997) and the present experiments and computations. From both of these comparisons it appears that the analogy between flow over a solid object and that generated by the motion of the time-varying surface shape of a gravity current is of some use but is not exact.

6. Discussion and conclusions

Certain characteristics of the propagation of lock-release gravity currents in a linearly stratified fluid have been measured. These include the Froude number of the initial constant velocity motion, the time and distance from the origin at which the

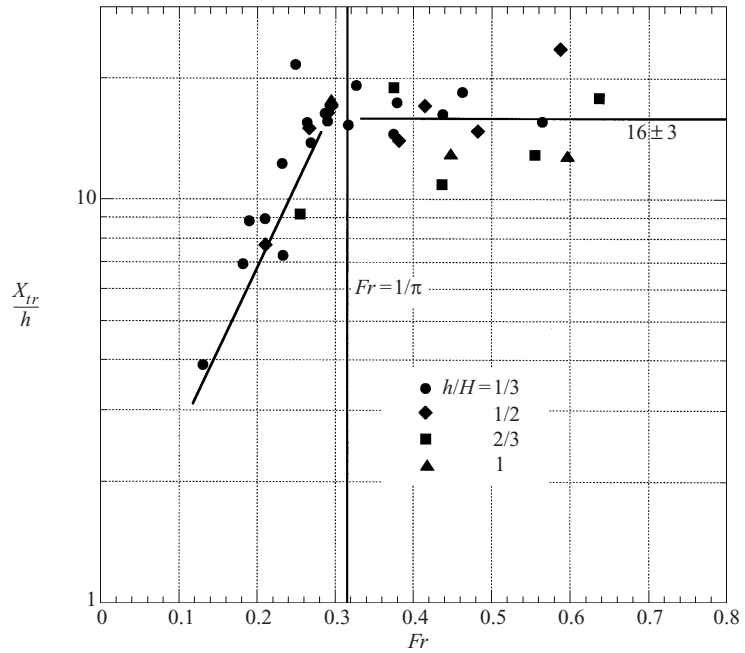

FIGURE 13. The dimensionless transition distance, X_{tr}/h versus Fr. Here, also, the solid lines have been added as a visual guide to the reader in order to show the data trend.

velocity begins to decrease and the regime in which a strong internal wave response is generated.

The initial, constant velocity, V, as measured by the Froude number, $Fr = V/NH$, has been found to have a simple dependence on the input parameters, ρ_b, ρ_C, ρ_0, h/H and L/h. For the ranges used here there appears to be no dependence on L/h. The first three parameters can be combined into the most significant dimensionless quantity:

$$R = N_C^2/N^2, \quad \text{where} \quad N_C^2 = g(\rho_C - \rho_0)/\rho_0 H, \quad N^2 = g(\rho_b - \rho_0)/\rho_0 H,$$

which removes the direct dependence on N and measures the relative strength of the current and density stratification. Then Fr depends logarithmically on R, over the range of R considered, while the coefficients of this dependence, C and K, vary logarithmically, or as a power law, with h/H. Thus once R and h/H are fixed a calculation of Fr follows immediately. Note however a slight deviation from this result for the two lowest values of h/H and R close to unity for both the physical and numerical experiments. We suspect that this is a real effect and not a result of experimental inaccuracies.

The characteristics of this initial motion are described well by a two-dimensional computation with a no-slip boundary condition. The appearance of the head of the current is very different from that seen in the experiments yet the quantitative agreement on front velocity between the two is remarkable. For a series of inviscid computations with a slip boundary condition (S. B. Dalziel, private communication) the agreement was not as good and suggests that experiments at a free surface, where the slip condition is likely to be more appropriate, should be carried out for comparison with the latter computations. Such experiments will be performed and reported in the future. These two observations suggest that while the details of head

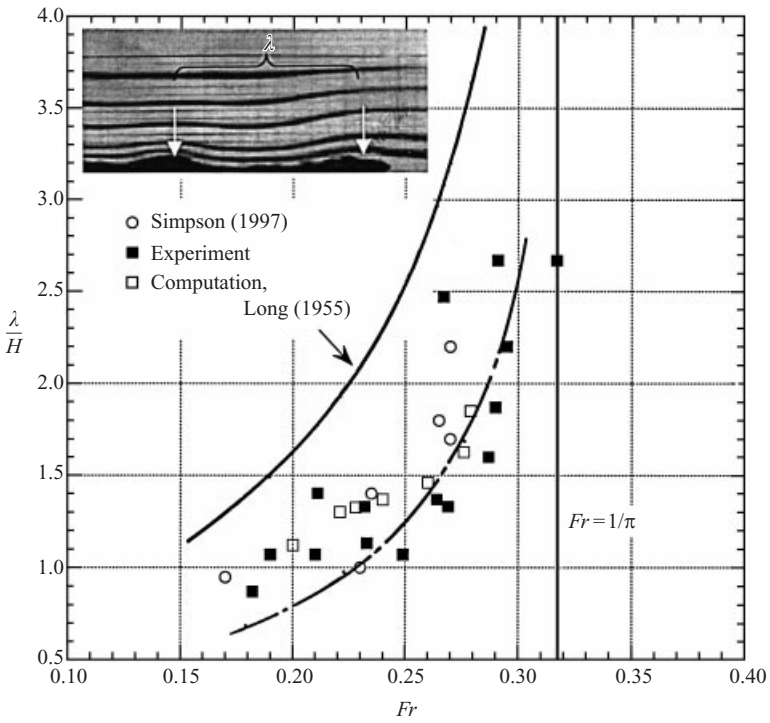

FIGURE 14. λ/H versus Fr for all available experimental and computational results. The definition of λ is shown in the photographic insert. Equation (11) is indicated as the Long (1955) curve. The chain-dotted line is shown as a guide to visualization and is given by Long's (1955) result divided by two. Note that in the present experiments waves were observed only when Fr was less than $1/\pi$.

structure are not important to a calculation of the gross features of the flow, the nature of the boundary condition at the wall is significant.

The results contained in equation (7)–(10) are of some interest. In particular, consider the limiting behaviour of C and K, and hence Fr, as h/H becomes small, for all values of R. In the case of equations (7) and (8) Fr becomes zero at a finite but very small, experimentally unobtainable, value of h/H, while for equations (9) and (10) it becomes zero only at $h/H = 0$. For all practical purposes the two results are, in fact, indistinguishable. It is not completely clear at this point whether this means that the actual Fr tends to zero or that the length of the region of constant velocity goes to zero with a finite Fr, i.e. a region of constant Fr can no longer be defined. The results shown in figures 12 and 13 suggest that both X_{tr} and T_{tr} are both tending to zero in this limit so that the later possibility is the one that is most likely to be correct. In turn, this observation suggests that it will not be possible to use the present results to calculate the constant-velocity phase of current motion at very small values of h/H except in the very restrictive way discussed above, i.e. for short distances and times only. Also, these results show that under all but the most extreme conditions the initial flow will be subcritical and will rapidly evolve to a state where wave motion and interactions are the most likely outcome. This state can only be described qualitatively by the work presented here, as for example in figure 6. Furthermore, the results shown in figure 11 suggest that equation (4) will also be inadequate and that the assumptions used to generate it will no longer hold in this same limit.

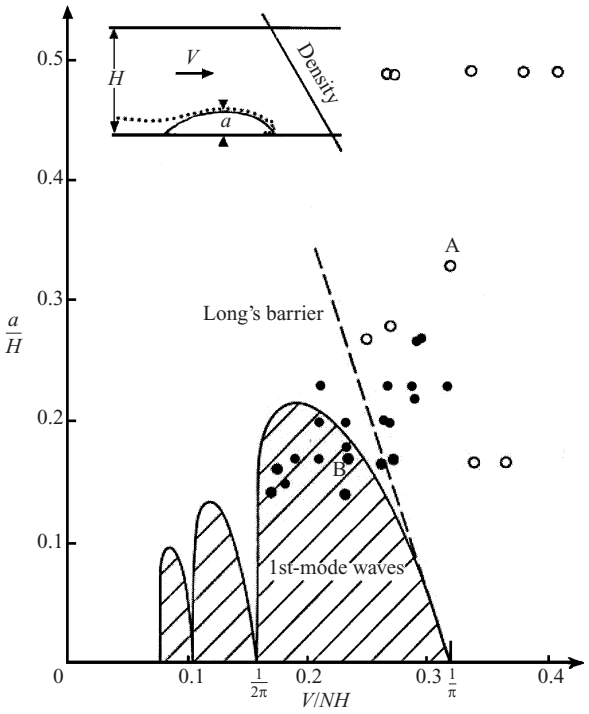

FIGURE 15. Regime diagram in $(a/H, V/NH)$ space for the existence of well-defined waves. The diagram itself and the black and open points are from Simpson (1997) and the details are described there. The smaller black points are from the present experiments. 'Long's Barrier' indicates the theoretical limit for wave generation over a solid object of finite amplitude. Note that the criterion $Fr \leqslant 1/\pi$ seems to be a better measure of the region in which waves can be generated by an object that changes shape as it propagates.

Further study of figures 12 and 13 shows quite clearly, as alluded to above, that the length of the dammed region (L), for the range considered, does not seem to play a role in determining the transition length, as it does in the classical case (Rottman & Simpson 1983). This is true even for large R where the constant-velocity regime appears to be approaching that of the classical gravity current. Now the appropriate length scale is the height of the damned region. There is a change in behaviour at the critical value of Fr. For supercritical, increasing Fr the transition distance remains a constant multiple of h while the transition time decreases. An explanation in terms of a reflected wave, as in the classical gravity current, is unlikely to be relevant. For the subcritical case both the dimensionless X_{tr} and T_{tr} increase with increasing Fr. The major difference between the two types of behaviour is that in the latter case the slowing is due to the interaction with the trough of the first generated wave, while in the former it appears to be due simply to the fact that an energetic primary wave has to be generated and this removes enough energy from the current itself to slow it. Based on this simple argument the trend of X_{tr} and T_{tr} in the subcritical regime can be rationalized. When Fr is small the wave generated by the initial release has a speed of order NH/π so that it quickly catches up with the slowly moving current, slows it further and X_{tr} and T_{tr} are small. As Fr increases, the difference between the current speed and the wave speed (which remains constant at NH/π) decreases so that X_{tr} and T_{tr} increase. As the two speeds approach equality,

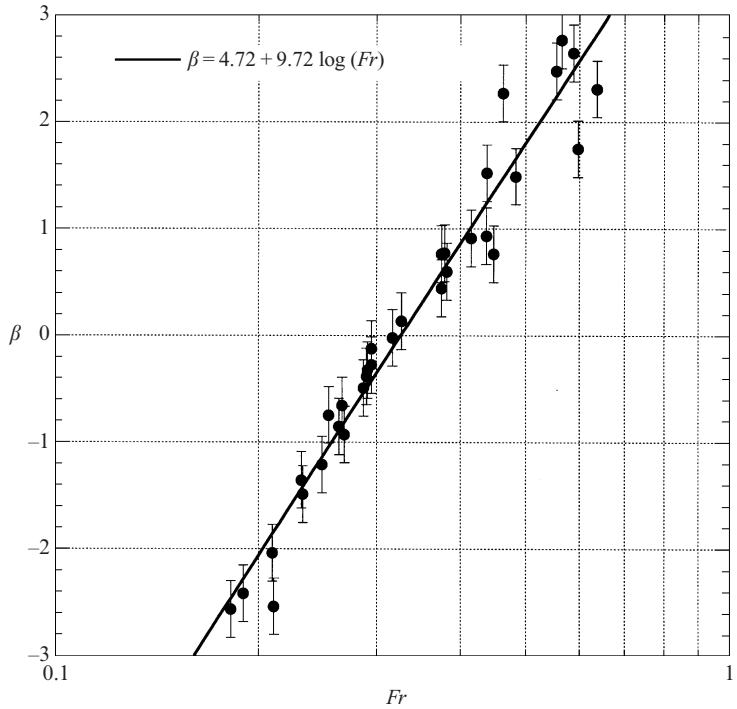

FIGURE 16. A plot of $\beta = (\pi Fr - 1)(H/a)$ vs. Fr (equation B1): a test for a possible solitary wave explanation of the observed behaviour of the gravity current.

i.e. Fr approaches $1/\pi$, this argument would suggest that the current speed would never change. Clearly other effects arise before this can happen and more detailed experiments are needed to sort out the relative importance of the various mechanisms discussed here.

Based on all of the results presented here it appears that the critical condition $Fr = 1/\pi$ delineates two regions of quite different flow. On the subcritical side, wave generation dominates the dynamical picture. The release of the current not only generates the waves but its subsequent motion is, in turn, greatly affected by them. On the other hand a release in the supercritical regime generates at least one initial wave but subsequent waves, if they exist, are weak and do not appear to affect further current motion. This latter statement is subject to possible revision since the experimental tank may not be long enough to observe all the interactions that might be possible in a longer one.

The work reported here was supported internally at the University of Southern California and University of Cambridge. (T. M. and J. L. would like to thank Professor Franz Durst, Director of the LSTM, Friedrich Alexander Universtät, Erlangen-Nürnberg, for his advice, help and encouragement during all phases of the work presented here. The comments of the referees and discussions with Professors H. Huppert of the University of Cambridge and M. Ungarish of the Technion, Haifa are acknowledged with thanks.

Appendix A

The experimental parameters are given in table 1.

Expt	h/H	$AR = L/h$	ρ_b	ρ_C	ρ_0	N	N_C	R	Fr	NT_{tr}	X_{tr}/h
1	2/3	2	1.032	1.035	1.004	1.351	1.421	1.107	0.255	24	9.18
2	2/3	2	1.033	1.045	1.004	1.374	1.634	1.414	0.375	33.7	18.96
3	2/3	2	1.035	1.090	1.005	1.397	2.352	2.833	0.637	18.7	17.87
4	1/3	4	1.044	1.070	1.005	1.593	2.057	1.667	0.317	16.1	15.31
5	1/3	4	1.037	1.119	1.003	1.489	2.750	3.412	0.565	9.2	15.59
6	1/3	4	1.034	1.075	1.004	1.398	2.151	2.367	0.438	12.4	16.29
7	1/3	4	1.034	1.065	1.004	1.398	1.993	2.033	0.375	12.9	14.51
8	1/3	4	1.033	1.037	1.005	1.350	1.443	1.143	0.182	12.7	6.93
9	1/3	4	1.033	1.049	1.005	1.350	1.702	1.589	0.290	18	15.66
10	1/3	4	1.036	1.045	1.003	1.467	1.655	1.273	0.232	17.6	12.25
11	1/3	4	1.034	1.034	1.003	1.422	1.422	1.000	0.131	9.9	3.89
12	1/3	4	1.035	1.048	1.004	1.421	1.703	1.435	0.269	17.1	13.80
13	2/3	4	1.064	1.099	1.008	1.907	2.433	1.629	0.437	16.6	10.88
14	2/3	2	1.065	1.139	1.008	1.932	2.917	2.280	0.555	15.5	12.90
15	1/3	4	1.065	1.094	1.006	1.958	2.390	1.490	0.287	19	16.36
16	1/3	4	1.064	1.072	1.006	1.942	2.080	1.147	0.190	15.5	8.84
17	1/3	4	1.067	1.112	1.005	2.001	2.638	1.738	0.327	19.6	19.23
18	1/3	4	1.066	1.163	1.008	1.945	3.170	2.655	0.463	13.3	18.47
19	1/3	4	1.065	1.088	1.007	1.941	2.294	1.397	0.264	19.6	15.52
20	1/3	4	1.065	1.122	1.006	1.958	2.746	1.966	0.379	15.3	17.40
21	1/3	4	1.067	1.082	1.006	2.000	2.235	1.249	0.233	10.4	7.27
22	1/3	4	1.067	1.079	1.006	2.000	2.181	1.189	0.210	14.2	8.95
23	1/3	8	1.068	1.085	1.008	1.965	2.232	1.291	0.249	29	21.66
24	1/2	8/3	1.067	1.069	1.008	1.948	1.983	1.036	0.211	18.3	7.72
25	1/2	8/3	1.066	1.082	1.008	1.940	2.202	1.288	0.295	28.9	17.05
26	1/2	8/3	1.067	1.115	1.008	1.957	2.639	1.819	0.415	20.6	17.10
27	1/2	8/3	1.069	1.181	1.007	2.007	3.363	2.808	0.588	20.1	23.64
28	1/2	8/3	1.035	1.042	1.004	1.410	1.582	1.259	0.291	28.2	16.41
29	1/2	8/3	1.035	1.040	1.003	1.444	1.555	1.159	0.267	28.1	15.01
30	1/2	16/3	1.036	1.054	1.003	1.456	1.827	1.575	0.382	18.3	13.98
31	1/2	8/3	1.068	1.139	1.007	1.990	2.927	2.162	0.483	15.3	14.78
32	1	4/3	1.068	1.072	1.009	1.947	2.019	1.075	0.295	60	17.70
33	1	8/3	1.068	1.104	1.007	1.990	2.505	1.584	0.448	29	12.99
34	1	4/3	1.034	1.072	1.004	1.386	2.103	2.302	0.597	21.5	12.84
35	1	4/3	1.034	1.094	1.004	1.398	2.421	3.000	0.701		
36	2/3	2	1.067	1.067	1.0075	1.965	1.965	1.000	0.230		

TABLE 1.

Appendix B. Test of a solitary wave explanation for the observed motion of the current head

It was thought that a different presentation of the velocity data might be possible based on the idea that the head wave, for the supercritical cases at least, was simply a large-amplitude, nonlinear internal solitary wave.† If this were true then it might be expected that, as in the cases of the KdV or Benjamin–Ono equations for example, a

† Note that unlike cases with a strongly nonlinear density distribution, as in e.g. Maxworthy (1980), a linear profile can only support solitary waves if non-Boussinesq effects are important. However, it was argued in Amen & Maxworthy (1980) that such effects seemed to explain their results. This suggestion is placed in doubt by the present results.

simple linear deviation from the long wave speed would be appropriate:

$$V = [NH/\pi][1 + \beta(a/H)]$$

or

$$\pi Fr = 1 + \beta(a/H),$$

where a is the amplitude or height of the gravity current head during the constant-velocity phase (see figure 15) and β should be a constant. The amplitudes of the waves were measured and $\beta = (\pi Fr - 1)(H/a)$ plotted against both R and Fr. Only plotting against Fr reduced the data in a consistent way, curiously, for both the sub- and supercritical cases (figure 16), so that

$$a/H = (\pi Fr - 1)/(4.72 + 9.72 \log_{10} Fr). \tag{B 1}$$

It is clear that the original conjecture that solitary wave ideas might explain the data is not correct, since not only is β not constant but the data reduction fits the subcritical results too. Finally, since both Fr and a/H are dependent variables this reduction can only be used in conjunction with equations (7)–(10) to calculate Fr, for given R and h/H, and then using equation (B1) to find a/H for the calculated Fr.

REFERENCES

Amen, R. & Maxworthy, T. 1980. The gravitational collapse of a mixed region into a linearly stratified fluid. *J. Fluid Mech.* **96**, 65–80.

Britter, R. E. & Simpson, J. E. 1978 Experiments on the dynamics of a gravity current head. *J. Fluid Mech.* **88**, 223–240.

Britter, R. E. & Simpson, J. E. 1981 A note on the structure of the head of an intrusive gravity current. *J. Fluid Mech.* **112**, 459–466.

Canuto, C., Hussani, M. Y., Quarteroni, A. & Zang, T. A. 1988 *Spectral Methods in Fluid Dynamics.* Springer.

Didden, N. & Maxworthy, T. 1982 The viscous spreading of plane and axisymmetric gravity currents. *J. Fluid Mech.* **121**, 27–42.

Felix, Y. 2000 An analytic model of gravity currents in a stable atmosphere. *J. Fluid Mech.* **420**, 27–46.

Härtel, C., Meiburg, E. & Necker, F. 2000 Analysis and direct numerical simulation of the flow at a gravity current head. Part I. Flow topology and front speed for slip and non-slip boundaries. *J. Fluid Mech.* **418**, 189–212.

Huppert, H. E. 1982 The propagation of two-dimensional and axisymmetric viscous gravity currents over a rigid, horizontal surface. *J. Fluid Mech.* **121**, 43–58.

Huppert, H. E. & Simpson, J. E. 1980 The slumping of gravity currents. *J. Fluid Mech.* **99**, 785–799.

Klemp, J. B., Rutunno, R. & Shamarock, W.C. 1994 On the dynamics of gravity currents in a channel. *J. Fluid Mech.* **269**, 169–198.

Leilich, J. 2000 Dynamics of gravity currents in a linearly stratified fluid. Diplomarbeit, LSTM, Friedrich Alexander Üniversität, Erlangen-Nürnberg and the University of South California.

Lele, S. K. 1992 Compact finite difference schemes with spectral-like resolution. *J. Comput. Phys.* **103**, 16–42.

Long, R. R. 1955 Some aspects of the flow of stratified fluids, III. Continuous density gradients. *Tellus.* **VII** (3), 341–357.

Manins, P. C. 1976 Intrusions into a stratified fluid. *J. Fluid Mech.* **74**, 547–560.

Maxworthy, T. 1980 On the formation of nonlinear internal waves from the gravitational collapse of mixed regions in dimensions. *J. Fluid Mech.* **96**, 47–64.

Oster, G. 1965 Density gradients. *Sci. Am.* **213** (2), 70–76.

Rottman, J. W. & Simpson, J. E. 1983 Gravity currents produced by instantaneous releases of a heavy fluid in a rectangular channel. *J. Fluid Mech.* **135**, 95–110.

SCHOOLEY, A. H. & HUGHES, B. A. 1972 An experimental and theoretical study of internal waves generated by the collapse of a two-dimensional mixed region in a density gradient. *J. Fluid Mech.* **51**, 159–175.

SIMPSON, J. E. 1972 Effects of the lower boundary on the head of a gravity current. *J. Fluid Mech.* **53**, 759–768.

SIMPSON, J. E. 1997 *Gravity Currents in the Environment and the Laboratory*, 2nd Edn. Cambridge University Press.

SIMPSON, J. E. & BRITTER, R. E. 1979 The dynamics of the head of a gravity current advancing over a horizontal surface. *J. Fluid Mech.* **94**, 477–495.

WRAY, A. A. 1991 Minimal storage time-advancement schemes for spectral methods. Preprint.

WU, J. 1969 Mixed region collapse with internal wave generation in a density-stratified medium. *J. Fluid Mech.* **35**, 531–544.